

See discussions, stats, and author profiles for this publication at: <https://www.researchgate.net/publication/278734283>

The order-disorder phase transition in lipid bilayers mediates a force for assembly of transmembrane proteins

Article · June 2015

Source: arXiv

CITATIONS

4

READS

289

5 authors, including:



Kranthi K Mandadapu

University of California, Berkeley

98 PUBLICATIONS 1,061 CITATIONS

[SEE PROFILE](#)



Berend - Smit

University of California, Berkeley

597 PUBLICATIONS 53,518 CITATIONS

[SEE PROFILE](#)

Some of the authors of this publication are also working on these related projects:



Active Matter -- (Statistical Mechanics, Continuum Mechanics and Applications) [View project](#)



Energy and environment materials [View project](#)

Pre-transition effects mediate forces of assembly between transmembrane proteins

Shachi Katira *¹, Kranthi K. Mandadapu ^{†‡§¹}, Suriyanarayanan Vaikuntanathan ^{§¹}, Berend Smit *^{‡¶} and David Chandler *

^{*}Department of Chemistry, University of California, Berkeley, CA 94720, USA, [†]Chemical Sciences Division, Lawrence Berkeley National Laboratory, Berkeley, CA 94720, USA, [‡]Department of Chemical and Biomolecular Engineering, University of California, Berkeley, CA 94720, USA, [§]Department of Chemistry, University of Chicago, Chicago, IL, 60637, USA, and [¶]Institut des Sciences et Ingénierie Chimiques, Valais Ecole Polytechnique Fédérale de Lausanne Rue de l'Industrie 17, Sion CH-1950 Switzerland

We present a mechanism for a generic and powerful force of assembly and mobility for transmembrane proteins in lipid bilayers. This force is a pre-transition (or pre-melting) effect for the first-order transition between ordered and disordered phases in the host membrane. Using large scale molecular simulation, we show that a protein with hydrophobic thickness equal to that of the disordered phase embedded in an ordered bilayer stabilizes a microscopic order-disorder interface, and the stiffness of that interface is finite. When two such proteins approach each other, they assemble because assembly reduces the net interfacial free energy. In analogy with the hydrophobic effect, we refer to this phenomenon as the “orderphobic effect.” The effect is mediated by proximity to the order-disorder phase transition and the size and hydrophobic mismatch of the protein. The strength and range of forces arising from the orderphobic effect are significantly larger than those that could arise from membrane elasticity for the membranes we examine.

lipid bilayers, phase transition, hydrophobic mismatch, orderphobe

Abbreviations: DPPC: dipalmitoyl phosphatidylcholine

This paper presents implications of the first-order order-disorder phase transition in lipid bilayers. The fluid mosaic model [1] and the lipid raft hypothesis [2] have guided intuition on how proteins diffuse in biological membranes — ordered clusters floating in an otherwise disordered fluid membrane [3, 4]. However, recent advances show that the state of membranes containing transmembrane proteins is ordered, even gel-like [5–10]. How then do transmembrane proteins diffuse and assemble within this relatively rigid material? Here, we argue that this question is answered by the fact that a transmembrane protein in an ordered bilayer can induce effects that resemble pre-melting [11–13]. Specifically, with molecular simulation, we show that within an otherwise ordered membrane phase, mesoscopic disordered domains surround proteins that favor disordered states. We find, importantly, that the boundary of the domains resembles a stable, fluctuating order-disorder interface. The dynamic equilibrium established at the boundary allows the protein and its surrounding domain to diffuse.

Moreover, because the interface has a finite stiffness, neighboring proteins can experience a membrane-induced force of adhesion, an attractive force that is distinctly stronger and can act over significantly larger lengths than those that can arise from simple elastic deformations of the membrane [14–18]. This force between transmembrane proteins is analogous to forces of interaction between hydrated hydrophobic objects. In particular, extended hydrophobic surfaces in water can nucleate vapor-liquid-like interfaces. In the presence of such interfaces, hydrophobic objects cluster to reduce the net interfacial free energy. This microscopic pre-transition effect manifesting the liquid-vapor phase transition can occur at ambient conditions [19–26].

In the transmembrane case, we show here that a protein favoring the disordered phase creates a similar pre-transition effect. In this case it manifests the order-disorder transition

of a lipid bilayer. Like the raft hypothesis, therefore, clusters do indeed form, but the mechanism for their assembly and mobility emerge as consequences of order-disorder interfaces in an otherwise ordered phase. We refer to this phenomenon as the “orderphobic effect.”

The order-disorder transition is a first-order phase transition. We choose the MARTINI model of hydrated dipalmitoyl phosphatidylcholine (DPPC) lipid bilayers [27] to illustrate the orderphobic effect. See *Methods*. This membrane model exhibits an ordered phase and a disordered phase. Fig. 1A contrasts configurations from the two phases, and it shows our estimated phase boundary between the two phases. The ordered phase has regular tail packing compared to the disorganized tail arrangement of the disordered phase. A consequence of the regular tail packing is that hydrophobic thickness of the ordered phase, D_o , is larger than that of the disordered phase, D_d . Correspondingly, the area per lipid in the ordered phase is smaller than that in the disordered phase.

Rendering the end particles of all the lipid chains in one of the two monolayers provides a convenient visual representation that distinguishes the two phases. These tail-end particles appear hexagonally-packed in the ordered phase and randomly arranged in the disordered phase. Regions that appear empty in this rendering are in fact typically filled by non tail-end particles or by tail-end particles from the other lipid monolayer.

Significance

The clustering of proteins in biological membranes is a controlling factor in processes such as endo- and exo-cytosis, cell signaling, and immunological synapses. Yet physical principles governing this organization are incompletely understood. Here, we address some of this uncertainty by demonstrating a general mechanism for mobility and powerful forces of assembly for transmembrane proteins.

Reserved for Publication Footnotes

¹ These authors contributed equally.

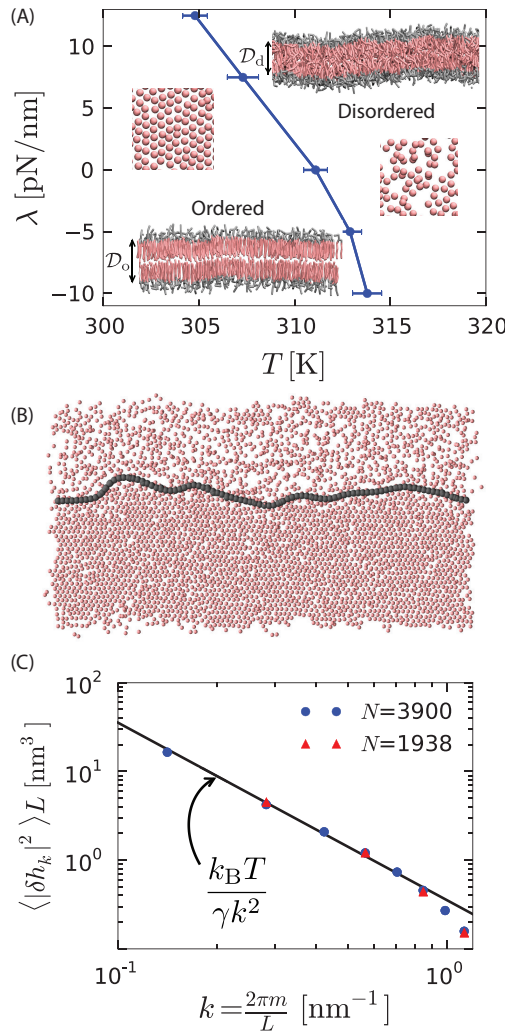


Fig. 1. (A) Order-disorder phase diagram in the tension–temperature, λ – T , plane. The lateral pressure across the membrane is $-\lambda$. Points are estimated from 10 independent heating runs like those illustrated in Fig. S1 for a periodic system with 128 lipids. Insets are cross sections showing configurations of a bilayer with 3200 lipids in the ordered and disordered phases. The heads are colored gray while the tails are colored pink. Water particles are omitted for clarity. The hydrophobic thicknesses, D_o and D_d , are the average vertical distances from the first tail particle of the upper monolayer to that of the lower monolayer. A macroscopic membrane buckles for all $\lambda < 0$. Snapshots of the last tail beads in one monolayer of each phase are shown to illustrate the difference in packing. (B) Snapshot of a system showing coexistence between the ordered and disordered phases. The gray contour line indicates the location of the interface separating the ordered and disordered regions. The snapshot is a top view of the bilayer showing the tail-end particles of each lipid in one monolayer. (C) Fourier spectrum of the fluctuations of the instantaneous order-disorder interface. The line is the small- k capillarity-theory behavior with $\gamma = 11.5 \text{ pN}$.

To quantify the distinctions between the two phases, we consider a local rotational-invariant [28–30], $\phi_l = |(1/6) \sum_{j \in nn(l)} \exp(6i\theta_{lj})|^2$, where θ_{lj} is the angle between an arbitrary axis and a vector connecting tail-end particle l to tail-end particle j , and the summation is over the six nearest neighbors of particle l . The equilibrium average, $\langle \phi_l \rangle$, is 1 for a perfect hexagonal packing, and it is 1/6 or smaller in the absence of bond-orientation correlations. Small periodically replicated samples of the DPPC hydrated membrane exhibit hysteretic changes in area per lipid and in $\langle \phi_l \rangle$ during heating and cooling. See *Supporting Information (SI)*, and Refs. [31]

and [32]. To establish whether the first-order-like behavior persists to large scales and thus actually manifests a phase transition, we consider larger systems and the behavior of the interface that separates the ordered and disordered phases.

Fig. 1B shows coexistence for a system size of $N = 3900$ lipids with an interface between the two phases. To analyze interfacial fluctuations, we first identify the location of the interface at each instant. This location is found with a two-dimensional version of the three-dimensional constructions described in Refs. [13] and [33]. Specifically, and as discussed in *Methods*, the interface is the line in the plane of the bilayer with an intermediate coarse-grained value of the orientational-order density,

$$\phi(\mathbf{r}) = \sum_l \phi_l \delta(\mathbf{r} - \mathbf{r}_l). \quad [1]$$

where \mathbf{r}_l is the position of the l th tail-end particle projected onto a plane parallel to that of the bilayer, \mathbf{r} is a two-dimensional vector specifying a position in that plane, and $\delta(\mathbf{r})$ is Dirac's delta function. We focus on this field rather than the tail-end number density, $\rho(r) = \sum_l \delta(\mathbf{r} - \mathbf{r}_l)$, because the difference between the two phases is larger for typical orientational-order than for typical tail-end density.

Fig. 1C shows the Fourier spectrum of the height fluctuations of this interface, $\langle |\delta h_k|^2 \rangle$. Two different system sizes are studied, with the larger system having approximately double the interface length of the smaller system. The Fourier component δh_k is related to the height fluctuation $\delta h(x)$ as $\delta h(x) = \sum_k \delta h_k \exp(ikx)$ where x is a point along the horizontal in Fig. 1B. Here, $0 \leq x \leq L$, and L is the box length. With periodic boundary conditions, $k = 2\pi m/L$, $m = 0, \pm 1, \pm 2, \dots$. According to capillarity theory for crystal–liquid interfaces [34,35], $\langle |\delta h_k|^2 \rangle \sim k_B T / L \gamma k^2$ for small k , with k_B being the Boltzmann's constant.

Given the proportionality with $1/k^2$ at small k (i.e., wavelengths larger than 10 nm), comparison of the proportionality constants from simulation and capillarity theory determines the interfacial stiffness, yielding $\gamma = 11.5 \pm 0.46 \text{ pN}$. This value is significantly larger than the prior estimate of interfacial stiffness for this model, $3 \pm 2 \text{ pN}$ [31]. That prior estimate was obtained from simulations of coarsening of the ordered phase.

Because the ordered phase has a hexagonal packing, the interfacial stiffness depends on the angle between the interface and the lattice of the ordered phase. For a hexagonal lattice, there are three symmetric orientations for which the interfacial stiffnesses are equal. We will see that for the model we have simulated there appears to be only little angle dependence. Irrespective of that angle dependence, the stability of the interface and the quantitative consistency with capillary scaling provide our evidence for the order–disorder transition being a first-order transition in the model we have simulated.

The system sizes we have considered contain up to 10^7 particles, allowing for membranes with $N \approx 10^4$ lipids, and requiring $10 \mu\text{s}$ to equilibrate. As such, our straightforward simulations are unable to determine whether the ordered phase is hexatic or crystal because correlation functions that would distinguish one from the other [36] require equilibrating systems at least 10 times larger [37]. Similarly, we are unable to determine the range of conditions for which the membranes organize with ripples and with tilted lipids [38,39]. Presumably, the ordered domain of the phase diagram in Fig. 1A, partitions into several subdomains coinciding with one or more of these possibilities. With advanced sampling techniques [40], free energy functions of characteristic order parameters can be computed to estimate the positions of boundaries between these various ordered behaviors. Here, we do not pursue this additional level of detail in the phase diagram because the ad-

ditional boundaries refer to *continuous* transitions [38]. It is only the first-order transition, with its *discontinuous* change between ordered and disordered phases, that supports coexistence with a finite interfacial stiffness, and it is this stiffness that results in the orderphobic effect, which we turn to now.

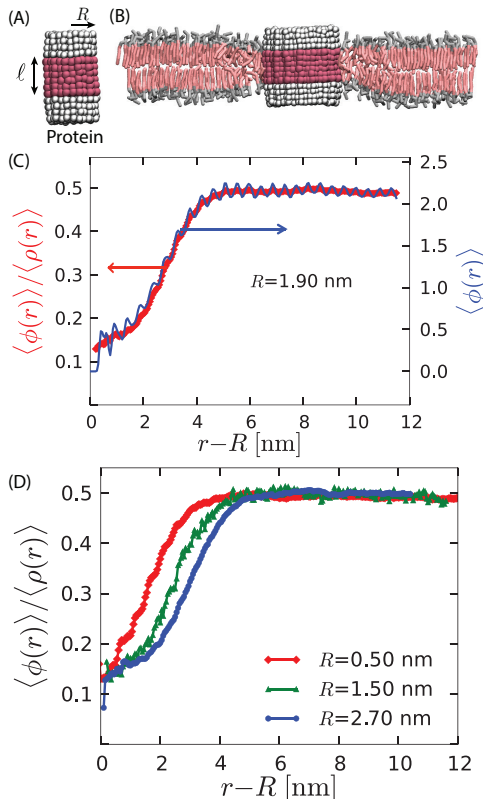


Fig. 2. Model proteins in the bilayer. (A) Idealized cylindrical protein-like solutes with radius R and hydrophobic thickness ℓ (magenta). The hydrophilic caps of the protein are shown in white. (B) Cross section of the lipid bilayer in the ordered phase containing a model protein of radius 2.7 nm with a hydrophobic thickness $\ell=2.3\text{ nm} \leq \mathcal{D}_d$. (C) The radial variation of the order parameters $\langle \phi(r) \rangle$ (right axis) and $\langle \phi(r) \rangle / \langle \rho(r) \rangle$ (left axis) show disorder in the vicinity of the protein of radius 1.9 nm. (D) Comparison of the radial order parameter variation for three different proteins shows an increase in the extent of the induced disorder region with protein radius.

Transmembrane proteins can disfavor the ordered membrane. A disordering (i.e., orderphobic) transmembrane protein is one that solvates more favorably in the disordered phase than in the ordered phase. The disordering effect of the protein could be produced by specific side chain structures. See SI. Here, in the main text, we consider a simpler mechanism. In particular, we have chosen to focus on the size of the protein's hydrophobic thickness and the extent to which that thickness matches the thickness of the membrane's hydrophobic layer [41, 42]. See Fig. 2.

The membrane's hydrophobic layer is thicker in the ordered state than in the disordered state. For instance, at zero lateral pressure and 294 K in the model DPPC membrane, we find that the average thicknesses of the hydrophobic layers in the ordered and disordered states are $\mathcal{D}_o = 3.1\text{ nm}$ and $\mathcal{D}_d = 2.6\text{ nm}$, respectively. A transmembrane protein with hydrophobic thickness of size $\ell \approx 2.6\text{ nm}$ will therefore favor the structure of the disordered phase. If the protein is large

enough, it can melt the ordered phase near the protein and result in the formation of an order-disorder interface.

Spatial variation of the order parameter field characterizes the spatial extent of the pre-melting layer. To evaluate whether a model protein is nucleating a disordered domain in its vicinity, we calculate the average of the orientational-order density field as a function of $r = |\mathbf{r}|$, $\langle \phi(r) \rangle$ (right axis of Fig. 2C). It exhibits oscillations manifesting the atomistic granularity of the system. Dividing by the mean density, $\langle \rho(r) \rangle$, largely removes these oscillations.

A profile of this ratio in the vicinity of the protein is depicted in Fig. 2C (left axis). It changes approximately sigmoidally, connecting its values of 0.15 and 0.45 in the disordered and ordered phases, respectively. The shape of the profile suggests the formation of an order-disorder interface [43]. Further, the increase in the spatial extent of the disordered region with the increasing size of the protein Fig. 2D is indicative of length scale dependent broadening effects brought about by capillary fluctuations. These impressions can be quantified by analyzing fluctuations of the instantaneous interface, which we turn to now.

An orderphobic protein nucleates a fluctuating order-disorder interface. Fig. 3A shows a configuration of the instantaneous interface that forms around the orderphobic protein shown in Fig. 2B. The interface is identified as described above. A video of its dynamics is provided at <https://goo.gl/NBQJP9>.

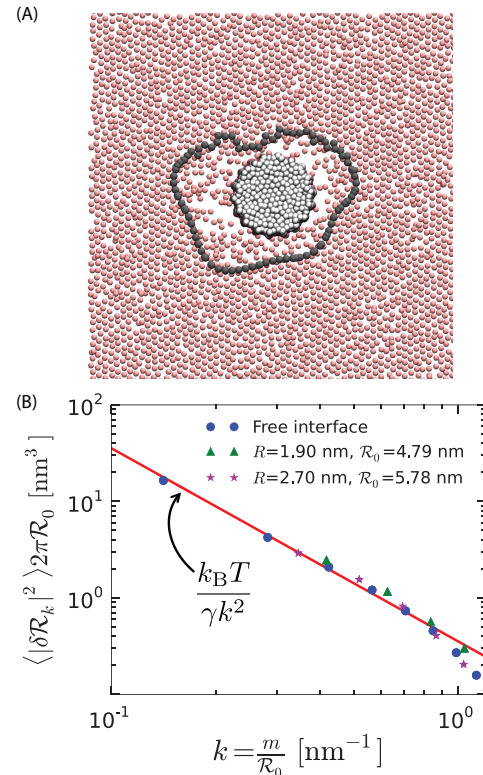


Fig. 3. Soft order-disorder interface: (A) Arrangement of the tail end particles of the top monolayer corresponding to the protein in Fig. 2B. Far away from the protein, the tail end particles show hexagonal-like packing and are in the ordered state. Proximal to the protein, it can be seen that the tail end particles are randomly arranged, and resemble the disordered phase. The line connected by the black points denotes the instantaneous order-disorder interface. (B) The fluctuations in the radius of the order-disorder interface are consistent with the fluctuations of a free order-disorder interface at coexistence. \mathcal{R}_0 is the mean radius of the order-disorder interface surrounding a model protein of radius R .

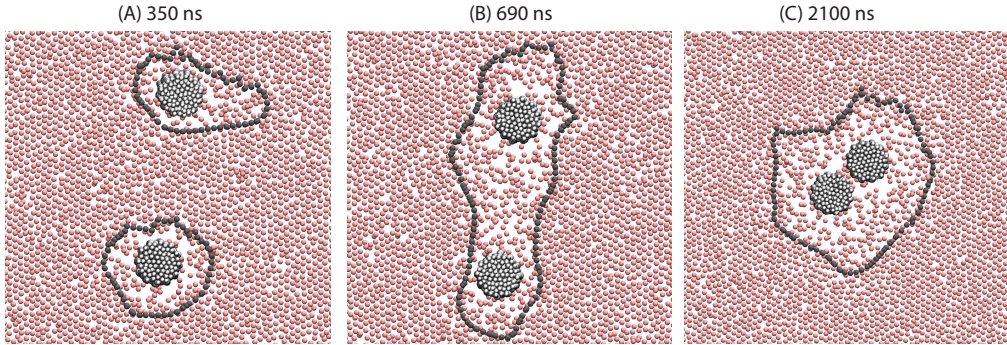


Fig. 4. Demonstration of the orderphobic force: Two proteins separated by a center-to-center distance of 14 nm are simulated at 309 K. Snapshots at various times reveal the process of assembly in which the two order-disorder interfaces merge into a single interface.

As is common in crystal–liquid interfaces, the interface nucleated by an orderphobic protein may exhibit hexagonal faceting [34], remnants of which can be observed in Fig. 3A.

The mean interface is a circle of radius \mathcal{R}_0 . Fourier analysis of fluctuations about that circle yields a spectrum of components. To the extent that these fluctuations obey statistics of capillary wave theory for circular interface, the mean-square fluctuation for the k th component is $\langle |\delta\mathcal{R}_k|^2 \rangle = k_B T / 2\pi\gamma k^2 \mathcal{R}_0$, where $k = m/\mathcal{R}_0$ and $m = \pm 1, \pm 2, \dots$, and γ is the order–disorder interfacial stiffness, neglecting the dependence on the angle between the interface and the lattice. The discrete values of k reflect periodic boundary conditions going full circle around the model protein.

In Fig. 3B, we use the interfacial stiffness from the free interface ($\gamma = 11.5$ pN) separating coexisting ordered and disordered phases with the capillary theory expression, and its corresponding spectrum, to compare with the spectrum of the protein-induced interface. The agreement between the theory, free interface and the protein-induced interface is good, and it improves as the radius of the orderphobic protein increases and the wave vector k decreases. This agreement indicates that the orderphobic protein does indeed nucleate an interface manifesting the order–disorder transition. The deviations of the fluctuations of the free interface from capillary wave theory occur for $k \gtrsim 0.8 \text{ nm}^{-1}$, corresponding to wavelengths $2\pi/k \lesssim 7 \text{ nm}$, and a mean interface radius $\mathcal{R}_0 \lesssim 1 \text{ nm}$. Indeed, Fig. 2 suggests that even a small protein of radius 0.5 nm, which supports an interface of radius $\mathcal{R}_0 \approx 1.2 \text{ nm}$, is sufficient to induce an order–disorder interface with fluctuations consistent with capillary theory.

The orderphobic effect generates forces of assembly and facilitates protein mobility. Fig. 4 shows three snapshots from a typical trajectory initiated with two orderphobic proteins of radius 1.5 nm separated by a distance of 14 nm. Each induces a disordered region in its vicinity, with soft interfaces separating the ordered and disordered regions. The free energy of the separated state is approximately $\gamma(P_1 + P_2)$, where P_i is the perimeter of the order–disorder interface around protein i . On average, $\langle P_i \rangle = 2\pi\mathcal{R}_0$. After a few hundred nanoseconds, a fluctuation occurs where the two interfaces combine. While the single large interface remains intact, the finite tension of the interface pulls the two proteins together. Eventually, the tension pulls the two proteins together with a final perimeter, P_f , that is typically much smaller than $P_1 + P_2$. A video of its dynamics is provided at <https://goo.gl/HXSOj7>.

After the separated interfaces join, the assembly process occurs on the time scale of microseconds. This time is required for the proteins to push away lipids that lie in the path of the assembling proteins. Given this time scale, a reversible work

calculation of the binding free energy would best control both the distance and the number of lipids between the proteins. Moreover, the evident role of interfacial fluctuations indicates that the transition state ensemble for assembly must involve and interplay between inter-protein separations and lipid ordering as well as lipid concentration.

While we leave the study of reversible work surfaces and transition state ensembles to future work, it seems already clear that the net driving force for assembly is large compared to thermal energies. For example, with a model orderphobic protein radius of 1.5 nm, we find $\gamma(\langle P_f \rangle - 2\langle P_1 \rangle) \approx -30 k_B T$. The range over which the force acts is given by the average radius of the two interfaces, $2\mathcal{R}_0$. This range is further amplified by the width of the interface, which is of $\mathcal{O}(\mathcal{R}_0)$ for one-dimensional interfaces in two-dimensional systems [44]. The typical range is ≈ 10 to 30 nm . In comparison, given the elastic moduli of the membranes we consider, elastic responses will generate attractive forces between transmembrane proteins that are much smaller in strength and range, typically $-5 k_B T$ and 1 nm, respectively [18, 45]. Moreover, similarly weak and short ranged forces are found from solvation theory that accounts for linear response in microscopic detail while not accounting for the possibility of an underlying phase transition [46].

As in the hydrophobic effect [19], the strength and range of the orderphobic force leverages the power of a phase transition, depending in this case on the ability of the orderphobic protein to induce a disordered layer in its vicinity. This ability depends upon the proximity to the membrane’s phase transition, and, for the simple protein models considered in this paper, it depends upon the protein’s radius and hydrophobic mismatch with the membrane. The spatial extent of the disordered region increases with proximity to phase coexistence as shown in Fig. 5A.

Furthermore, Fig. 5B shows that the strength of the effect is maximal for a hydrophobic thickness equal to that of the disordered phase, and it decreases as the hydrophobic thickness approaches that of the ordered phase. In the case of zero mismatch, i.e., $\ell = \mathcal{D}_o$, the value of the order parameter in the vicinity of the protein is consistent with that of a pure bilayer in the ordered state. Therefore, the model proteins with zero mismatch, do not induce a disordered region, and the orderphobic effect vanishes. See Figs. 5B and 5D.

Fig. 4 also shows that the orderphobic effect produces excess mobility, by proteins melting order in a surrounding microscopic layer and by facilitating the motions of neighboring proteins. This finding explains how protein mobility and reorganization can be relatively facile in the so-called “gel” phases of membranes. Further information on this phenomenon is provided in *SI*. Our prediction of enhanced lipid mobility sur-

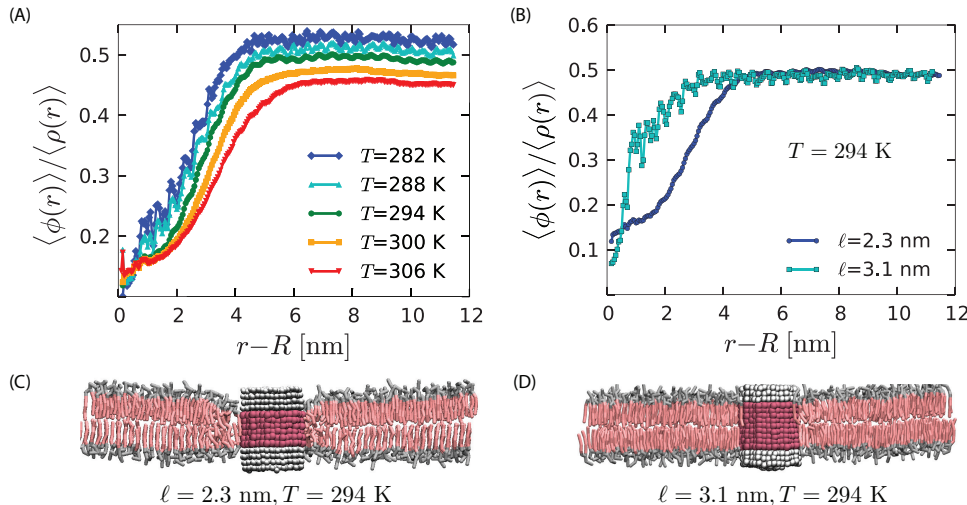


Fig. 5. Strength of the orderphobic force: (A) Radial variation of the order parameter showing the extent of the disordered region as a function of temperature, for a protein of radius 1.9 nm and hydrophobic thickness 2.3 nm. The extent of the disordered region increases as the melting temperature is approached, at zero surface tension. (B) Comparison of the radial variation of the order parameter for different hydrophobic mismatches. Proteins with no mismatch do not create any disordered region. (C) Arrangement of lipids around a protein with negative mismatch. (D) Arrangement of lipids around a protein with zero mismatch.

rounding orderphobic proteins may be amenable to experimental tests by single molecule tracking techniques [47].

Implications of the orderphobic effect and related phenomena in biological membranes. Biological membranes and transmembrane proteins are far more complicated than the models considered in this paper. Part of the complexity is associated with multiple components, which can be studied outside of biological contexts. For example, we anticipate that the orderphobic effect will be useful in understanding the phase behavior that results from mixing cholesterol with pure or multicomponent lipid bilayers [48–51]. In this case, cholesterol with small hydrophilic heads and short hydrophobic tails has the propensity to induce disorder in the ordered phase [50].

Transmembrane proteins in biological membranes have structures more complicated than those of our simple model proteins. The side chains of these proteins can affect the packing of lipid chains. To the extent that lipid packing is disrupted, even small α -helix proteins can be orderphobic. Evidence for this assessment is provided in SI. How associated orderphobic effects lead to clustering and related phenomena for transmembrane α -helices merit future study.

Further, there is a dual to the orderphobic effect: A transmembrane protein in the disordered phase that favors the ordered phase can nucleate an ordered region and order-disorder interface. For example, one of our model proteins with a positive mismatch ($\ell = D_o$) would induce order in its vicinity. Interfaces separating the ordered and disordered regions will again provide a force for assembly. This case corresponds to the situation of lipid rafts [2], which consists of ordered domains floating in otherwise disordered membranes.

Finally, we speculate that the orderphobic effect plays important roles in membrane fusion and cell signaling [52–55]. In the case of fusion, it would appear that one important role is to promote fluctuations in an otherwise stable membrane. Otherwise, it is difficult to conceive of a mechanism by which thermal agitation would be sufficient to destabilize microscopic sections of membranes. Such destabilization seems necessary for initiating and facilitating membrane fusion. Many proteins are involved in such processes [52, 56, 57], but it may not be a coincidence that the hydrophobic thicknesses of SNARE

proteins are 25% smaller than that of the ordered membrane states [58, 59].

Materials and Methods

Molecular simulations. We simulate the MARTINI coarse-grained force field using the GROMACS molecular dynamics package [27, 60]. ‘Antifreeze’ particles are added to the solvent to ensure that the solvent does not freeze over the temperature range considered in the simulations as in Ref. [27]. Thermostats and barostats control temperature and pressure, and checks were performed to assure that different thermostats and barostats yielded similar results [40]. The hydrophobic cores of our idealized proteins are constructed using the same coarse-grained beads as the lipid tails (particle C1 in the MARTINI topology [27]). Similarly, the hydrophilic caps are constructed using the first bead of the DPPC head group (Q0, in the MARTINI topology). The protein beads also have bonded interactions where the bond length is 0.45 nm and the bond angle is set to 180° . The associated harmonic force constants for the bond lengths and angles are $1250 \text{ kJmol}^{-1} \text{ nm}^{-2}$ and $25 \text{ kJmol}^{-1} \text{ rad}^{-2}$. Based on the hydrophobic mismatch with the bilayers, the proteins are classified into three categories: (i) positive mismatch ($\ell > D_o$) (ii) negative mismatch ($\ell \leq D_d$) and (iii) no mismatch ($\ell \approx D_o$). To create different mismatches, we alter the number of beads in the protein core. These idealized proteins do not contain charges.

Proteins are embedded in the equilibrated bilayer at 279 K. The resulting system is then heated to the required temperature and equilibrated for another $1.2 \mu\text{s}$. All the subsequent averages are performed using 10 independent trajectories each 600 ns long. The assembly of proteins is also performed using the same DPPC bilayer system with 3200 lipids and 50000 water beads. In this case, two proteins are inserted in this bilayer with centers at a distance of 14 nm and the simulation is carried out at 309 K.

The flat interface is stabilized by juxtaposing an ordered bilayer equilibrated at 285 K and zero lateral pressure with a disordered bilayer equilibrated at the same conditions corresponding to the cooling and heating curves of the hysteresis loop in Fig. S1, respectively. The system thus constructed is equilibrated in the ensemble with fixed temperature, volume and numbers of particles. This ensemble allows for maintaining an area per lipid intermediate between the two phases, thus stabilizing the interface.

Instantaneous interface. For the purpose of obtaining a smooth and continuous interface, $\phi(\mathbf{r})$ is coarse grained by replacing Dirac’s delta function with a finite-width Gaussian, $(1/2\pi\xi^2) \exp(-|\mathbf{r}|^2/2\xi^2)$. The replacement changes $\phi(\mathbf{r})$ to $\bar{\phi}(\mathbf{r})$. The coarse-graining width, ξ , is chosen to be the average separation between tail-end particles i and j when $\langle (\phi_i - \langle \phi_i \rangle)(\phi_j - \langle \phi_j \rangle) \rangle / \langle (\phi_i - \langle \phi_i \rangle)^2 \rangle$ in the ordered phase is 1/10. This choice yields a value of $\xi=1.5 \text{ nm}$. The instantaneous order-disorder interface is the set of points \mathbf{s} satisfying $\bar{\phi}(\mathbf{s}, t) = (\phi_d + \phi_o)/2$. Here, ϕ_d and ϕ_o are $\langle \phi(\mathbf{r}) \rangle$ evaluated in the

disordered and ordered phases, respectively. At zero lateral pressure and 294 K, we find $\phi_d = 0.4 \pm 0.02 \text{ nm}^{-2}$ and $\phi_o = 2.15 \pm 0.2 \text{ nm}^{-2}$. For numerics, a square lattice tiles the average plane of the bilayer, and the coarse-grained field $\bar{\phi}(\mathbf{r})$ is evaluated at each lattice node. Values between are determined by interpolation. For convenience, the Gaussian function is truncated and shifted to zero at 3ξ . Any value of ξ within the range, $1 \text{ nm} < \xi < 2 \text{ nm}$ gives nearly identical $\bar{\phi}(\mathbf{r})$. Outside that range, larger values obscure detail by excessive smoothing, and smaller values obscure detail by capturing a high density of short-lived bubbles of disorder.

ACKNOWLEDGMENTS. It is a pleasure to thank Axel T. Brunger, Jay Groves and John Kuriyan for helpful conversations about this work, and Tom Lubensky and Siewert-Jan Marrink for helpful comments on earlier drafts of this work. SV is currently supported by the University of Chicago. In the initial stages, he was supported by Director, Office of Science, Office of Basic Energy Sciences, Materials Sciences, and Engineering Division, of the U.S. Department of Energy under contract No. DE AC02-05CH11231. KKM, DC, SK and BS are supported by that same DOE funding source, the latter two with FWP number SISGRKN. This research used resources of the National Energy Research Scientific Computing Center, a DOE Office of Science User Facility supported by the Office of Science of the U.S. Department of Energy under Contract No. DE-AC02-05CH11231 and resources of the Midway-RCC computing cluster at University of Chicago.

1. Singer, S. J & Nicholson, G. L. (1972) The fluid-mosaic model of the structure of cell membranes. *Science* 175:720–731.
2. Simons, K & Ikonen, E. (1997) Functional rafts in cell membranes. *Nature* 387:569–572.
3. Simons, K & Toomre, D. (2000) Lipid rafts and signal transduction. *Nat Rev Mol Cell Biol* 1:31–39.
4. Lingwood, D & Simons, K. (2010) Lipid rafts as a membrane-organizing principle. *Science* 327:46–50.
5. Nishimura, S. Y., Vrljic, M., Klein, L. O., McConnell, H. M & Moerner, W. E. (2006) Cholesterol depletion induces solid-like regions in the plasma membrane. *Biophys J* 90:927–938.
6. Polozov, I. V., Bezrukova, L., Gawrisch, K & Zimmerberg, J. (2008) Progressive ordering with decreasing temperature of the phospholipids of influenza virus. *Nat Chem Biol* 4:248–255.
7. Swamy, M. J et al. (2006) Coexisting domains in the plasma membranes of live cells characterized by spin-label ESR spectroscopy. *Biophys J* 90:4452–4465.
8. Munro, S. (2003) Lipid rafts: elusive or illusive? *Cell* 115:377–388.
9. Thewalt, J. L & Bloom, M. (1992) Phosphatidylcholine cholesterol phase diagrams. *Biophys J* 63:1176–1181.
10. Owen, D. M., Williamson, D. J., Magenau, A & Gaus, K. (2012) Sub-resolution lipid domains exist in the plasma membrane and regulate protein diffusion and distribution. *Nat Commun* 3:1–7:1256.
11. Lipowsky, R. (1982) Critical surface phenomena at first-order bulk transitions. *Phys Rev Lett* 49:1575.
12. Lipowsky, R. (1984) Surface-induced order and disorder: Critical phenomena at first-order phase transitions. *J Appl Phys* 55:2485–2490.
13. Limmer, D. T & Chandler, D. (2014) Premelting, fluctuations, and coarse-graining of water-ice interfaces. *J Chem Phys* 141:18C505.
14. Dan, N., Pincus, P & Safran, S. A. (1993) Membrane-induced interactions between inclusions. *Langmuir* 9:2768–2771.
15. Goulian, M., Bruinsma, R & Pincus, P. (1993) Long-range forces in heterogeneous fluid membranes. *Europhys Lett* 22:145–150.
16. Phillips, R., Ursell, T., Wiggins, P. & Sens, P. (2009) Emerging roles for lipids in shaping membrane-protein function. *Nature* 459:379–385.
17. Kim, K. S., Neu, J. & Oster, G. (1998) Curvature-mediated interactions between membrane proteins. *Biophys J* 75:2274–2291.
18. Haselwandter, C. A & Phillips, R. (2013) Directional interactions and cooperativity between mechanosensitive membrane proteins. *Europhys Lett* 101:68001–1–6.
19. Chandler, D. (2005) Interfaces and the driving force of hydrophobic assembly. *Nature* 437:640–647.
20. Lum, K., Chandler, D & Weeks, J. D. (1999) Hydrophobicity at small and large length scales. *J Phys Chem B* 103:4570–4577.
21. Willard, A. P & Chandler, D. (2008) The role of solvent fluctuations in hydrophobic assembly. *J Phys Chem B* 112:6187–6192.
22. Stillinger, F. H. (1973) Structure in aqueous solutions of nonpolar solutes from the standpoint of scaled-particle theory. *J Solution Chem* 2:141–158.
23. ten Wolde, P. R & Chandler, D. (2002) Drying-induced hydrophobic polymer collapse. *Proc Natl Acad Sci USA* 99:6539–6543.
24. Mittal, J. & Hummer, G. (2008) Static and dynamic correlations in water at hydrophobic interfaces. *Proc Natl Acad Sci USA* 105:20130–20135.
25. Patel, A. J et al. (2011) Extended surfaces modulate hydrophobic interactions of neighboring solutes. *Proc Natl Acad Sci USA* 108:17678–17683.
26. Patel, A. J et al. (2012) Sitting at the edge: How biomolecules use hydrophobicity to tune their interactions and function. *J Phys Chem B* 116:2498–2503.
27. Marrink, S. J., Risselada, H. J., Yefimov, S. Y., Tieleman, D. P. & de Vries, A. H. (2007) The MARTINI force field: Coarse grained model for bimolecular simulations. *J Phys Chem B* 111:7812–7824.
28. Nelson, D. R. (2002) Defects and Geometry in Condensed Matter Physics. (Cambridge University Press).
29. Halperin, B. I & Nelson, D. R. (1978) Theory of two-dimensional melting. *Phys Rev Lett* 41:121–124.
30. Frenkel, D., Hanson, F. E. & McTague, J. P. (1980) Phase Transitions and Orientational Order in a Two Dimensional Lennard-Jones System. Springer, 285–292.
31. Marrink, S. J., Risselada, H. J. & Mark, A. E. (2005) Simulation of gel phase formation and melting in lipid bilayers using a coarse grained model. *Chem Phys Lipids* 135:223–244.
32. Rodgers, J. M., Sorensen, J., de Meyer, F. J.-M., Schiott, B. & Smit, B. (2012) Understanding the phase behavior of coarse-grained model lipid bilayers through computational calorimetry. *J Phys Chem B* 116:1551–1569.
33. Willard, A. P & Chandler, D. (2010) Instantaneous liquid interfaces. *J Phys Chem B* 114:1954–1958.
34. Nozières, P. (1992) Shape and growth of crystals. Solids far from equilibrium, Cambridge University Press, Cambridge 56:1–154.
35. Fisher, M. P. A. & Fisher, D. S. & Weeks, J. D. (1982) Agreement of capillary-wave theory with exact results for the interface profile of the two-dimensional Ising model. *Phys Rev Lett* 48:368.
36. Nelson, D. R., Rubinstein, M. & Spaepen, F. (1982) Order in two-dimensional binary random arrays. *Philosophical Magazine A* 46:105–126.
37. Bernard, E. P. & Krauth, W. (2011) Two-step melting in two dimensions: First-order liquid-hexatic transition. *Physical Review Letters* 107:155704.
38. Sirota, E. B., Smith, G. S., Safinya, C. R., Plano, R. J. & Clark, N. A. (1988) X-ray scattering studies of aligned, stacked surfactant membranes. *Science* 242:1406–1409.
39. Smith, G., Sirota, E., Safinya, C., Plano, R. & Clark, N. (1990) X-ray structural studies of freely suspended hydrated DMPC multimembrane films. *J Chem Phys* 92:4519–4529.
40. Frenkel, D & Smit, B. (2001) Understanding molecular simulation: from algorithms to applications. Academic Press.
41. Killian, J. A. (1998) Hydrophobic mismatch between proteins and lipids in membranes. *Biochim Biophys Acta* 1376:401–416.
42. Sharpe, H. J., Stevens, T. & Munro, S. (2010) A comprehensive analysis of transmembrane domains reveals organelle-specific properties. *Cell* 142:158–169.
43. Rowlinson, J. S. & Widom, B. (1982) Molecular theory of capillarity. (Clarendon Press: Oxford).
44. Kardar, M. 2007 Statistical Physics of Fields. Cambridge University Press.
45. De Meyer, F. J. -M., Venturoli, M. & Smit, B. (2008) Molecular simulations of lipid-mediated protein-protein interactions. *Biophys J* 95:1851–1865.
46. Lagüe, P., Zuckermann, M. J. & Roux, B. (1998) Protein inclusion in lipid membranes: a theory based on the hypernetted chain integral equation. *Faraday Discuss* 111:165–172.
47. Eggeling, C. et al. (2009) Direct observation of the nanoscale dynamics of membrane lipids in a living cell. *Nat Chem Biol* 457:1159–1162.
48. Ipsen, J. H., Karlstrom, G., Mouritsen, O. G., Wennerstrom, H. & Zuckermann, M. J. (1987) Phase equilibria in the phosphatidylcholine-cholesterol system. *Biochim Biophys Acta* 905:162–172.
49. Risselada, H. J. & Marrink, S. J. (2008) The molecular face of lipid rafts in model membranes. *Proc Natl Acad Sci USA* 105:17367–17372.
50. Sodt, A. J., Sandar, M. L., Gawrisch, K., Pastor, R. W. & Lyman, E. (2014) The molecular structure of the liquid-ordered phase of lipid bilayers. *J Am Chem Soc* 136:725–732.
51. Radhakrishnan, A. & McConnell, H. M. (2005) Condensed complexes in vesicles containing cholesterol and phospholipids. *Proc Natl Acad Sci USA* 102:12662–12666.
52. Fratti, R. A., Jun, Y., Merz, A. J., Margolis, N. & Wickner, W. (2004) Interdependent assembly of specific regulatory lipids and membrane fusion proteins into the vertex ring domain of docked vacuoles. *J Cell Biol* 167:1087–1098.
53. Zick, M., Stroupe, C., Orr, A., Douville, D. & Wickner, W. T. (2014) Membranes linked by trans-SNARE complexes require lipids prone to non-bilayer structure for progression to fusion. *Elife* 3:e01879.
54. Qi, S. Y., Groves, J. T. & Chakraborty, A. K. (2001) Synaptic pattern formation during cellular recognition. *Proc Natl Acad Sci USA* 98:6548–6553.
55. James, J. R. & Vale, R. D. (2012) Biophysical mechanism of T-cell receptor triggering in a reconstituted system. *Nature* 487:64–69.
56. Fasshauer, D., Bryan Sutton, R., Brunger, A. T & Jahn, R. (1998) Conserved structural features of the synaptic fusion complex: SNARE proteins reclassified as Q- and R-SNAREs. *Proc Natl Acad Sci USA* 95:15781–15786.
57. Wickner, W. & Schekman, R. (2008) Membrane fusion. *Nat Struct Mol Biol* 15:658–664.
58. Milovanovic, D. et al. (2015) Hydrophobic mismatch sorts SNARE proteins into distinct membrane domains. *Nat Commun* 6:5894.
59. Stein, A., Weber, G., Wahl, M. C. & Jahn, R. (2015) Helical extension of the neuronal SNARE complex into the membrane. *Nature* 460:525–528.
60. Pronk, S. et al. (2013) GROMACS 4.5: A high-throughput and highly parallel open source molecular simulation toolkit. *Bioinformatics* 29:845–854.
61. Korlach, J. et al. (1999) Characterization of lipid bilayer phases by confocal microscopy and fluorescence correlation spectroscopy. *Proc Natl Acad Sci USA* 96:8461–8466.
62. Schäfer, L. V. et al. (2011) Lipid packing drives the segregation of transmembrane helices into disordered lipid domains in model membranes. *Proc Natl Acad Sci USA* 108:1343–1348.

Supporting Information

for “... force for assembly of transmembrane proteins”

by Shachi Katira, Kranthi K. Mandadapu, Suriyanarayanan Vaikuntanathan, Berend Smit and David Chandler

In this Supporting Information, we examine hysteresis in the bilayer system, show results for mean-square displacements as functions of time, and provide evidence that a small transmembrane α -helix protein can be orderphobic if the side chains of the protein disrupt the packing of lipid tails.

The lipid bilayer system exhibits hysteresis

Fig. S1A shows the change in area per lipid with temperature while heating and cooling a bilayer. There are finite jumps in area per lipid as the system transitions between the two phases, suggesting a first-order phase transition. Hysteresis occurs because ordering from the metastable disordered phase is much slower than disordering from the metastable ordered phase. Due to the difference in time scales, when contrasting melting and freezing from heating and cooling runs, the melting points from heating runs as shown in Fig. 1A provide the more accurate estimates of the actual phase boundaries. Systematic errors due to small system size and heating rate have not been estimated.

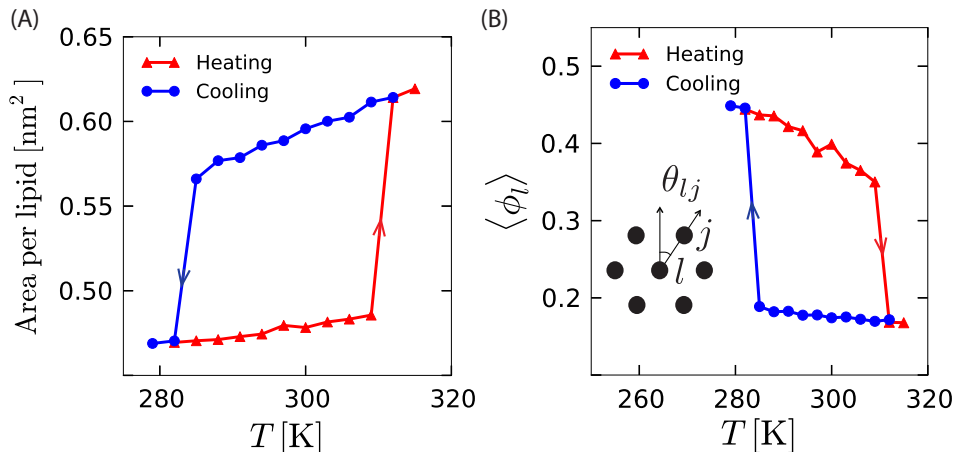


Fig. S1. Structural measures of different phases as a function of temperature, T . (A) Variation in area per lipid with temperature during heating and cooling shows finite jumps and hysteresis. (B) Average local orientational order, $\langle \phi_l \rangle$, also shows finite jumps as a function of temperature while heating and cooling. Magnitudes of heating and cooling rates are $3 \text{ K}/\mu\text{s}$.

The pre-melting layer has a higher mobility than the ordered phase

In Fig. S2 we show the mean squared displacements of lipids in the bulk ordered phase, bulk disordered phase, and the pre-melting layer induced by an orderphobic protein. As discussed in the main text, an orderphobic protein increases the mobility of the lipids in its vicinity. Note that the center of mass of the membrane fluctuates in time. These fluctuations affect the absolute positions of lipid molecules, but they are irrelevant to the issue of lipid mobility. Therefore, the mean-square displacements considered in Fig. S2 are for tail-end particle positions relative to the instantaneous position of the membrane's center of mass. That is to say, for $\langle |\bar{\mathbf{r}}_l(t) - \bar{\mathbf{r}}_l(0)|^2 \rangle$, where $\bar{\mathbf{r}}_l(t)$ is the position at time t of the l th tail-end particle less that of the membrane's center of mass.

For large enough times, t , the mean-square displacements are asymptotic to $4Dt$, where D is the self-diffusion constant. For the disordered liquid phase, we see from Fig. S2 that the asymptotic region is reached within 10^2 ns, and that $D \approx 4 \times 10^{-7} \text{ cm}^2/\text{s}$. In contrast, for the ordered phase, the diffusive asymptotic limit is not reached until 10^4 ns, and $D \approx 2 \times 10^{-9} \text{ cm}^2/\text{s}$. The mobility of lipids within the disordered layer surrounding the orderphobic protein is an order of magnitude larger than that of lipids beyond that region and in the ordered phase.

Experimental results for lipid diffusion constants in disordered and ordered bilayers are $D \approx 3 \times 10^{-8} \text{ cm}^2/\text{s}$ and $D \approx 2 \times 10^{-10} \text{ cm}^2/\text{s}$, respectively [61]. The simulation is in harmony with experiment for the two-order of magnitude difference between the ordered- and disordered-phase values of D . Of course, absolute values of D are beyond the scope of what can be predicted from our simulations because coarse graining omits degrees of freedom that would increase friction and decrease D .

A model α -helix is orderphobic

Here, we consider the MARTINI model for KALP23 — a polypeptide chain with 23 residues, consisting of alanines and leucines flanked by lysines [62]. This molecule has a hydrophobic thickness of $\ell \approx 3.0 \text{ nm}$, which means that it has essentially no

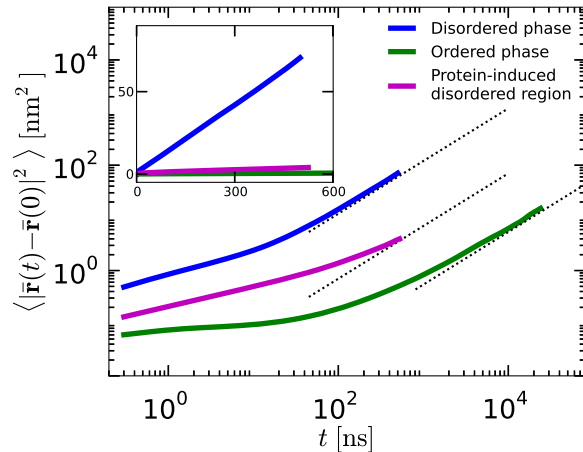


Fig. S2. Mean-square displacements as functions of time, t , for lipids in the disordered phase, the protein induced disordered domain, and the ordered phase. The functions are shown on log-log scale (main graphs) and linear scales (inset).

hydrophobic-length mismatch with the ordered bilayer. Nevertheless, it is orderphobic because its side chains perturb the ordered lipid phase to an extent that a pre-melting layer is formed around the protein. This behavior is demonstrated with the aid of Fig. S3. The panels render configurations from a simulation in which we have placed this model protein in the MARTINI model for the ordered DPPC bilayer system considered in the main text. The pre-melting layer that forms around the protein causes the protein to tilt so as to keep its full hydrophobic length in contact with hydrophobic tails of the lipids. The interface separating its disordered domain from the surrounding ordered phase remains stable throughout a molecular dynamics trajectory running for more than 1 μ s.

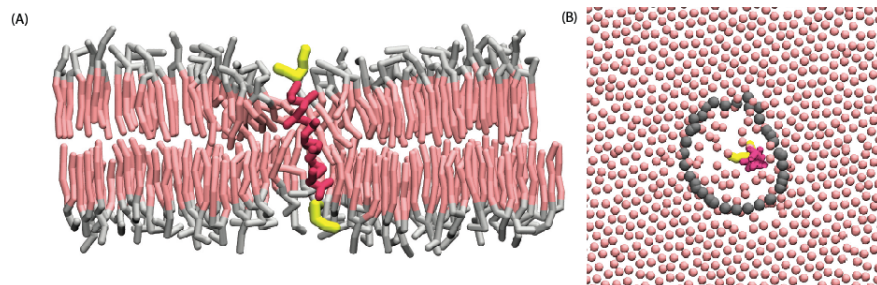


Fig. S3. A model α -helix is orderphobic. (A) Cross section of ordered phase of a hydrated DPPC membrane containing one transmembrane KALP23 protein. Solvent water is not rendered for purpose of clarity. Configuration was obtained after running simulation for roughly 1 μ s at 294 K and zero lateral pressure. (B) Configuration of tail-end particles for the top monolayer, with grey points locating the instantaneous interface.